Effect of liquidlike cations on electronic and defect properties of solid solutions of Cu_2Te and Ag_2Te

Xiaowei Wu [1], Chen Ming,[1] Weiwei Gao,[2] Jing Shi,[3] Kunpeng Zhao,[4] Han Wang,[5] and Yi-Yang Sun [1,*]

[1]*State Key Laboratory of High Performance Ceramics and Superfine Microstructure, Shanghai Institute of Ceramics, Chinese Academy of Sciences, Shanghai 201899, China*
[2]*Key Laboratory of Materials Modification by Laser, Ion and Electron Beams, Ministry of Education, Dalian University of Technology, Dalian 116024, China*
[3]*Department of Physics, Jiangxi Normal University, Nanchang 330022, China*
[4]*State Key Laboratory of Metal Matrix Composites, School of Materials Science and Engineering, Shanghai Jiao Tong University, Shanghai 200240, China*
[5]*Chemical Sciences Division, Lawrence Berkeley National Laboratory, Berkeley, California 94720, USA*

Cu_2Te was recently shown to be an excellent thermoelectric material with a figure of merit approaching 2. Ag alloying was found to be effective for tuning the electrical conductivity of Cu_2Te toward high thermoelectric performance. The liquidlike behavior of cations is well-known to yield ultralow thermal conductivity in the cuprous chalcogenide materials. Here, we study the effect of the liquidlike behavior on the electronic and defect properties of the solid solutions $Cu_{2-x}Ag_xTe$. Using first-principles molecular dynamics (MD) simulation, we found that the band-gap variation with increasing x as obtained from MD ensemble averages is much slower than that from direct calculation using the high-symmetry ordered structures. The solid solutions within the whole range of x exhibit significant band gaps. The liquidlike behavior also results in flattened top valence bands, which reduce the Seebeck coefficient and electrical conductivity. Regarding the defect properties, we found that the liquidlike behavior can fail the standard defect models employing the high-symmetry ordered structure. Again, MD simulation would be necessary for sampling the configuration space in defect calculations. However, converging the defect formation energy for the diffusive system would require much longer simulation time than converging the band gap. Our present results suggest that Ag alloying could slightly increase the formation energy of Cu vacancy.

I. INTRODUCTION

Cuprous chalcogenides (Cu_2X with X=S, Se, and Te) are excellent thermoelectric (TE) materials [1–12] owing to their liquidlike behavior of the copper cations, which gives rise to exceptionally low lattice thermal conductivity of 0.35 W m^{-1} K^{-1} even for Cu_2S with the relatively light elements [5,13]. Given the low thermal conductivity, the engineering toward high TE figure of merit (ZT) often focuses on tuning the electrical conductivity of these materials, which are all self-doped p-type semiconductors. Recent studies revealed that undoped Cu_2Se already has nearly optimal carrier concentration for high ZT. In comparison, Cu_2S is usually underdoped, while Cu_2Te is overly self-doped [11]. Purposely introducing Cu vacancies is employed to increase hole concentration in Cu_2S [5] while Ag alloying is identified to be an excellent way of reducing the hole concentration in Cu_2Te [4,11].

The ZT values of the Cu_2X compounds are all approaching or beyond 2 [7–11]. Compositing with other materials, such as carbon nanotubes and $CuInSe_2$, can further enhance the ZT to around 2.5 [14,15]. To further develop the potential of these materials, studies have been devoted to understanding their complex microstructures and phase changes [16–18]. Partly due to the unclear crystal structures, the electronic structures

of Cu_2X are also elusive and intriguing. For example, regarding the band gaps of Cu_2X in the cubic antifluoritelike (AF) structure, from density functional theory (DFT) calculations [19] they do not follow a monotonic trend with increased atomic number of the cation elements. Instead, Cu_2Se appears to have the smallest band gap, which is followed by Cu_2S. Surprisingly, Cu_2Te has the largest band gap. Also, the band gap of Cu_2Te has been predicted to be indirect, while Cu_2S and Cu_2Se are both direct. For Cu_2Se, even in a hybrid functional calculation it cannot open a band gap. While the modified Becke-Johnson (mBJ) potential amended by Hubbard U of 4 eV can open a gap of 0.50 eV, it has been suspected that the calculated band gap is still underestimated compared with that deduced from experiments [19]. On the experimental side, it is understandably difficult to measure the band gaps of the high-temperature phases. Early studies reported the band gap of Cu_2Te to be 0.7 to 1.2 eV [20–23]. But the measurements were done at room temperature, at which the material is not in the AF phase as characterized by x-ray diffraction (XRD) peaks around 12º.

Ag alloying has been identified as an approach to reducing the electrical conductivity of Cu_2Te to the optimal value so a balance between the high power factor and low carrier thermal conductivity can be achieved [11]. The effect of Ag alloying has been studied by DFT calculations [11]. It was found that Ag alloying can increase the formation energy of Cu vacancy, which reduces the hole concentration and in turn the electrical

*yysun@mail.sic.ac.cn

conductivity. However, the obtained formation energy of Cu vacancy was negative, indicating thermodynamic instability of the material. Alloying has also been explored to enhance the TE performance of Ag_2Te [24–26]. A ZT value of about 1.4 has been achieved by Cu alloying. Band gaps of the solid solutions have been measured at 673 K. Pure Ag_2Te exhibits a small band gap of around 0.23 eV [26]. In this paper, the mBJ + U method was again adopted in the DFT calculations, which yielded a band gap of 0.21 eV without considering the spin-orbit coupling (SOC) effect [26]. For Ag_2Te, however, the SOC could be strong enough to close the 0.21 eV band gap.

Because the mBJ potential is only applicable to static calculations on electronic structure and cannot be used for structural relaxation and molecular dynamics (MD) simulation, the previous calculations on Cu_2Te and Ag_2Te solid solutions were all conducted using the high-symmetry ordered structures without considering the liquidlike behavior of the cations. In this paper, based on MD simulations, we study the effects of liquidlike behavior of cations on electronic structures and defect properties of the solid solutions of Cu_2Te and Ag_2Te.

II. METHODS

All calculations were carried out with the VIENNA AB INITIO SIMULATION PACKAGE (VASP) [27]. The interaction between ion cores and valence electrons were described by projector augmented wave (PAW) potentials [28,29]. Semilocal (Perdew–Burke–Ernzerhof, PBE) [30] and hybrid (Heyd-Scuseria-Ernzerhof, HSE) [31] exchange-correlation functionals were adopted. In the HSE functional, the mixing parameter controlling the amount of Hartree-Fock (HF) exchange energy was set to 0.25. A rotationally invariant approach [32] to implementing the Hubbard U was adopted here to better describe the on-site Coulomb interactions among Cu $3d$ and Ag $4d$ electrons. The SOC effect was included in VASP by evaluating the Hamiltonian $\sigma \cdot \mathbf{L}$ within the PAW spheres.

To identify the U values for the Cu $3d$ orbitals, we performed linear response calculations [33]. Figure 1(a) shows the number of d electrons (N) on a selected Cu atom in a supercell as a function of the applied U value from -0.2 to 0.2 eV. One set of data was obtained using non-self-consistent (non-SCF) calculations with preconverged charge density from the case of $U = 0$ eV. From a linear fitting, one can obtain the non-SCF response function $\chi_0 = \partial N / \partial U |_{\text{non-SCF}}$. The other set of data was obtained using SCF calculations from which one can obtain the SCF response function $\chi = \partial N / \partial U |_{\text{SCF}}$. Then, the final U value was obtained by $U = 1/\chi - 1/\chi_0$. Different supercell sizes were checked to ensure the converged U value. The results are shown in Fig. 1(a), where it can be seen that for Cu_2Te the U value of Cu $3d$ orbitals converges to about 7 eV. Similar calculations were carried out for Ag_2Te in the same structure and yielded U of 2 eV for Ag $4d$ orbitals [Fig. 1(b)], significantly smaller than that for Cu $3d$ orbitals.

The cutoff energy for the plane-wave basis set was set to be 306 eV. When optimizing lattice constants, the cutoff energy was set to be 544 eV. The Brillouin zone for the cubic unit
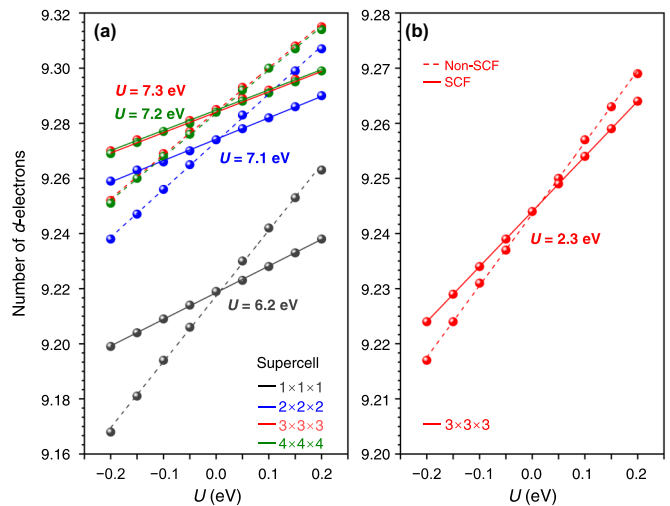

FIG. 1. Number of d electrons remaining on a Cu or Ag cation as a function of the applied U value for evaluating the Hubbard-U values of Cu $3d$ and Ag $4d$ orbitals in Cu_2Te (a) and Ag_2Te (b), respectively, by a linear response method. Dashed lines are from non-SCF calculations and solid lines are from SCF calculations. For Cu_2Te, different supercells were employed to check the convergence. It was found that a $3 \times 3 \times 3$ supercell is sufficiently large and was used in the calculation for Ag_2Te.

cell of AF-phase Cu_2Te and Ag_2Te was sampled by $4 \times 4 \times 4$ Γ-centered k points. A $2 \times 2 \times 2$ supercell containing 96 atoms was used for defect calculations and first-principles MD simulations. For the supercell, $2 \times 2 \times 2$ Γ-centered k points were used, which is necessary for converging the calculated defect formation energies to within 0.1 eV.

MD simulations was conducted based on the PBE + U method. Velocity scaling method was used to ramp the temperature up to 850 K. After that, the simulations were conducted with the NVT ensemble using a Nosé thermostat [34,35]. The time step was set to 1.25 fs. Thermal equilibration was done by running the simulation at 850 K for 10 ps (8000 steps).

Frequency calculations on the defect supercell were conducted by a finite-difference approach with an atomic displacement of 0.015 Å. All atoms in the supercell were allowed to move. Phonon calculations on bulk Cu_2Te were conducted using the PHONOPY package with a $2 \times 2 \times 2$ supercell [36]. Dynamical matrix was constructed by collecting the forces calculated by finite difference.

The electrical conductivity and Seebeck coefficient were calculated based on the Boltzmann transport theory as implemented in the TRANSOPTICS code [37–39]. A $14 \times 14 \times 14$ k-point mesh was used in the calculations of the electronic structure. The approximation of constant relaxation time was used in the calculation of electrical conductivity.

III. RESULTS AND DISCUSSION

A. High-symmetry $Fm\bar{3}m$ structure

Stoichiometric Cu_2Te exists in six phases from room temperature up to the melting point [40,41]. Several crystal structures have been proposed based on experimental
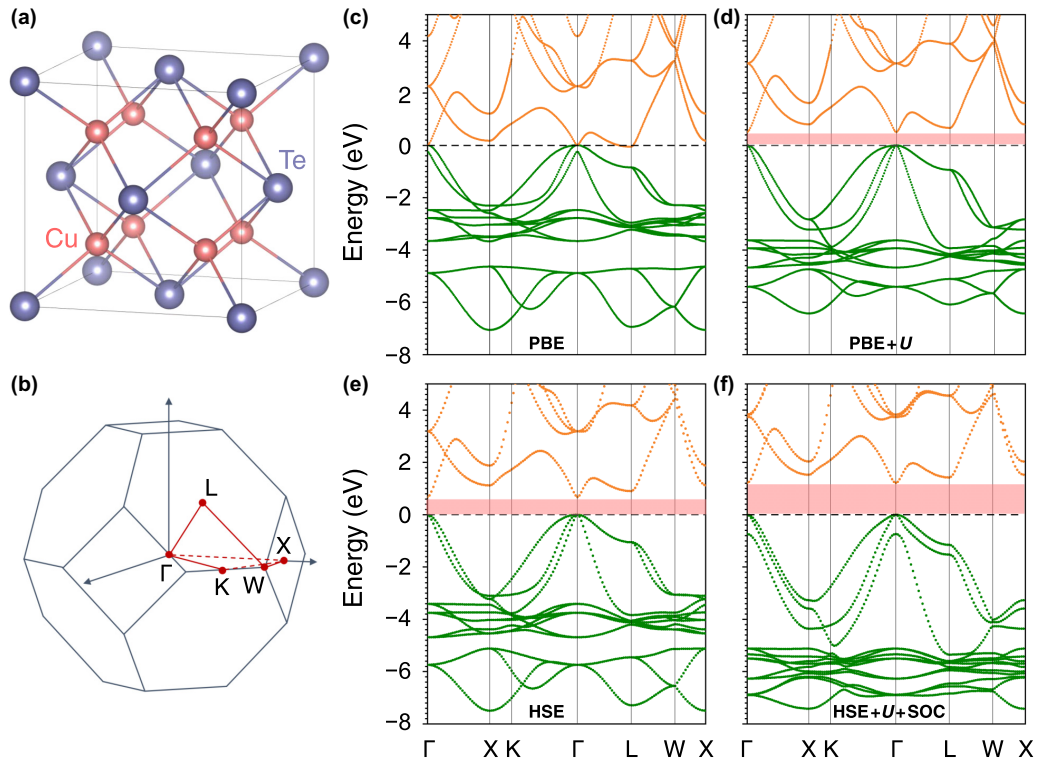
FIG. 2. (a) Crystal structure of high-symmetry ordered Cu_2Te with space group $Fm\bar{3}m$. (b) First Brillouin zone of Cu_2Te with high-symmetry k points. (c)–(f) Calculated band structure of Cu_2Te using the PBE, PBE $+ U$, HSE, and HSE $+ U +$ SOC methods, respectively.

measurements and theoretical computations [42,43]. However, none of them can well match measured XRD patterns [44] except for the AF phase, which is typically obtained above 840 K and characterized by the absence of XRD peaks below 20° [11]. It is possible that the low-temperature phases are not pure phases, but superstructures of mixed phases. This paper focuses on the AF phase as the highest ZT values were all observed in this phase.

In the AF phase, the anions form an fcc sublattice, while the cations are liquidlike. To show the effect of the liquidlike cations, however, we first calculated the band structure of Cu_2Te in the high-symmetry ordered structure (space group No. 225, $Fm\bar{3}m$) as shown in Fig. 2(a). The k points used in the band-structure plots are shown in Fig. 2(b). Using the PBE functional, we obtained a semimetallic band structure as shown in Fig. 2(c). At the Γ point, the triply degenerate valence band maximum (VBM) is slightly higher than the nondegenerate conduction band minimum (CBM) by about 0.1 eV, which will be referred to as a negative band gap below. As PBE is well-known to underestimate the band gap for typical semiconductors, we adopted the Hubbard-U approach and hybrid HSE functional to address the band-gap issue.

Using the PBE $+ U$ method with $U = 7$ eV, a band gap of 0.51 eV is opened at the Γ point as shown in Fig. 2(d). It should be noted that the Hubbard-U approach is to address the on-site Coulomb interaction of electrons in localized orbitals rather than a means of tuning the band gap [45]. Simply applying the PBE $+ U$ approach is usually not sufficient to obtain the experimental band gap. We further carried out calculations using the hybrid HSE functional, which yields more accurate band gaps for typical semiconductors. As shown in

Fig. 2(e), a band gap of 0.68 eV was obtained using the HSE functional, which is slightly larger than that from the PBE $+ U$ calculation. Considering the SOC effect, the band gap is reduced to 0.47 eV in HSE $+$ SOC calculations. Using $U = 7$ eV to carry out HSE $+ U +$ SOC calculation, we obtained a band gap of 1.22 eV, as shown in the band structure in Fig. 2(f). Note that the band gap is still direct, i.e., the conduction band valley at the Γ point is lower than that at the L point, which is different from the previous calculation using mBJ $+ U$ calculations [19]. The gap value is close to the upper bound of the experimentally measured results of 0.7–1.2 eV at room temperature [20–23]. The SOC splitting of the triply degenerate VBM states is 0.74 eV, as can be seen in Fig. 2(f). The doubly degenerate states are pushed up by 0.26 eV, while the single split-off state is pushed down by 0.49 eV.

B. Effect of liquidlike cations on band structure

To better show the effect of liquidlike cations, it is more illustrative to see the trend of band gaps of the $Cu_{2-x}Ag_xTe$ solid solutions. We considered regular occupation of Ag in the Cu sublattice. In the cubic unit cell of Cu_2Te, there are eight Cu atoms. We replaced them by Ag atoms one by one, while still preserving a space group belonging to the cubic crystal system. Thus, we can obtain the lattice constant for each composition by directly performing variable volume optimization. Figure 3(a) shows the variation of the lattice constant of $Cu_{2-x}Ag_xTe$ from PBE, PBE $+ U$, and HSE calculations. It can be seen that the lattice constant follows Vegard's law, i.e., increases linearly with the increase of Ag content. HSE calculations yield the smallest lattice constants. PBE
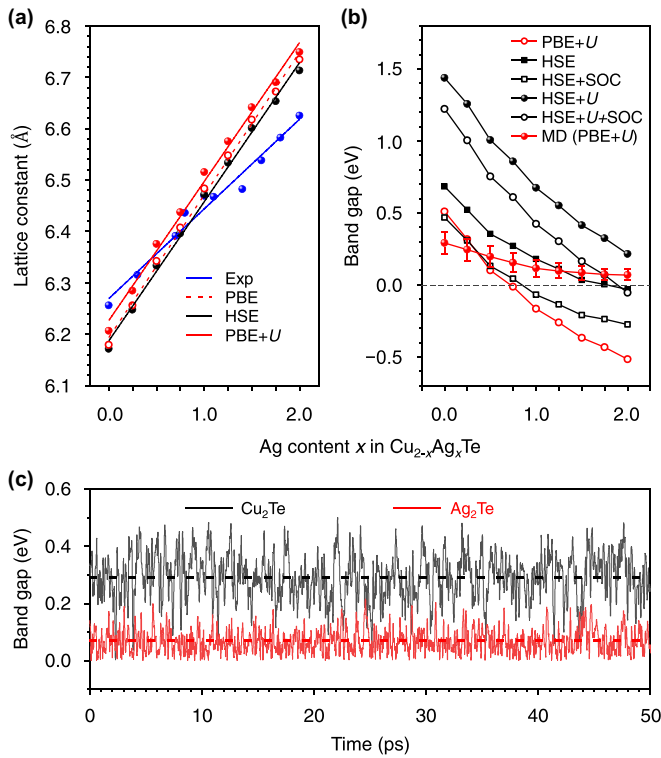
FIG. 3. (a) Lattice constant of $Cu_{2-x}Ag_xTe$ as a function of Ag content using different calculation methods. The experimental data are taken from Refs. [11,25,26]. (b) Band gap of $Cu_{2-x}Ag_xTe$ as a function of Ag content x using different calculation methods. The MD simulations were carried out with the PBE $+ U$ method. (c) Variation of the band gap with MD simulation time for Cu_2Te and Ag_2Te at 850 K. The dashed lines show the averaged values. The standard deviations evaluated from (c) were used as error bars for the MD results in (b).

calculations increase the lattice constants slightly, which are further increased in PBE $+ U$ calculations. However, the differences are all smaller than 0.7%. For comparison, Fig. 3(a) also shows the lattice constants collected from experimental measurements [11,25,26]. It can be seen that on the Cu-rich side, the calculations underestimate the lattice constants, while on the Ag-rich side the calculations overestimate the lattice constants. The largest errors for Cu_2Te and Ag_2Te are 1.4% and 1.9%, respectively. Figure 3(b) shows the variation of the band gap with Ag content calculated by PBE $+ U$, HSE, HSE $+$ SOC, HSE $+ U$, and HSE $+ U +$ SOC methods. Different from the lattice constant in Fig. 3(a), the band gap does not follow Vegard's law but exhibits slight downward bowing. The results from the most sophisticated HSE $+ U +$ SOC calculations are expected to be the most accurate results, except that the U value used here might be overestimated as the mixing of 25% Hartree-Fock exchange has corrected the on-site Coulomb interaction to some extent.

One discrepancy with the experimental results is that Ag_2Te was measured with a small band gap around 0.23 eV [26] while most of the calculations yielded negative band gaps for Ag_2Te. We conjecture that the liquidlike behavior of cations might be responsible for this discrepancy. To support this conjecture, we carried out MD simulations to evaluate the

effect of liquidlike behavior of Cu cations on the band gap. PBE $+ U$ method with $U = 7$ eV for Cu $3d$ and $U = 2$ eV for Ag $4d$ orbitals were used in the MD simulations. We obtained the band gap for each composition by averaging over 50 ps of simulation, which was after 10-ps thermal equilibration. Figure 3(b) shows the trend in the band gap with increasing Ag content. It can be seen that the band gaps from the MD simulations indeed exhibit slower variation (i.e., smaller slope) than those from the static calculations using the same PBE $+ U$ method (the two red-color lines). We checked that the averaged band gaps over 50-ps simulations converge to ± 0.01 eV, which give rise to a rather smooth curve for the MD results in Fig. 3(b). As examples, the variations of band gaps with simulation time for the cases of Cu_2Te and Ag_2Te at 850 K are shown in Fig. 3(c). It can be seen that the variation in the case of Cu_2Te is larger than that in the case of Ag_2Te. We calculated the standard deviations and used them as error bars in Fig. 3(b) for the MD results.

To understand the effect of the liquidlike behavior of cations on the electronic properties, we compared the band structures of the ordered structures with the $Fm\bar{3}m$ symmetry and the disordered structures from the MD simulations. The MD snapshots were chosen to exhibit the average band gaps for Cu_2Te and Ag_2Te, respectively. As can be seen in Figs. 4(a)–4(d) for both Cu_2Te and Ag_2Te, the band structures undergo a substantial change in the disordered structure. The top valence bands become much less dispersive than those of the high-symmetry ordered structures, indicating weaker hybridization of the atomic orbitals contributing to the top valence bands. Figures 4(e) and 4(f) show the charge density plots of the VBM states of the disordered structures, where it can be seen that the Te $5p$ and Cu $3d$ states are mostly separated without bonding. The charge density plots of the CBM states show that they are also contributed from the Te $5p$ and Cu $3d$ states. The only difference is that in Cu_2Te the CBM state shows significant hybridization between different atoms, which is responsible for the large variation of the CBM state during the MD simulation, as shown in Fig. 3(c).

C. Effect of liquidlike cations on thermoelectrics

Breaking the symmetry (or the ordered structure) leads to weak hybridization in top valence bands and hence the reduced band dispersion (or flattened top valence bands), which could profoundly affect the TE properties of the materials. Taking pristine Cu_2Te as an example, we calculated the electrical conductivity σ and Seebeck coefficient S as a function of hole concentration. The results are shown in Fig. 5. As constant relaxation time was employed in the calculation of σ, Fig. 5(a) shows the ratio of σ / τ with τ being the relaxation time. From Fig. 5, it is seen that the disordered structure yields consistently lower σ and S than the high-symmetry ordered structure. The lowered σ is caused by the flattened top valence band and, therefore, the increased hole effective mass. The lowered Seebeck coefficient is caused by the lift of degeneracy at the VBM due to the symmetry breaking. Overall, the disorder caused by liquidlike cations tends to reduce the power factor (i.e., $S^2\sigma$).

It is worthy noting that the high-symmetry $Fm\bar{3}m$ structure does not exist in reality. Instead, it is an averaged
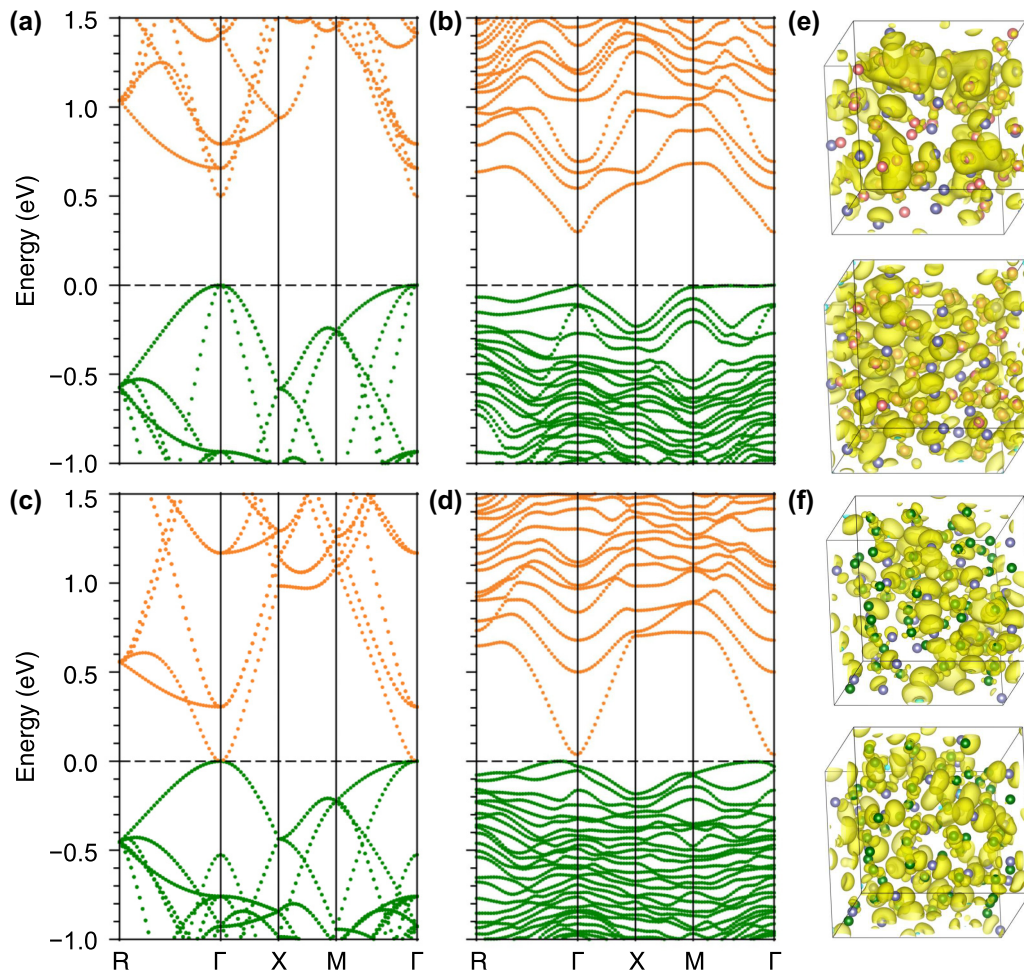
FIG. 4. Band structures of Cu_2Te obtained from a $2 \times 2 \times 2$ supercell in (a) the high-symmetry ordered structure with the $Fm\bar{3}m$ space group and (b) a symmetry-broken disordered structure from a snapshot in the MD simulation. (c) and (d) are similar to (a) and (b), respectively, but for Ag_2Te. (e) Charge density plots of CBM (upper panel) and VBM (lower panel) states corresponding to the band structure in (b). (f) Charge density plots of CBM (upper panel) and VBM (lower panel) states corresponding to the band structure in (d).

structure obtained from diffraction measurements, which typically capture signals over a timescale several orders of magnitude longer than that for the hopping of Cu ions. As the electronic structure of the material at each time snapshot is significantly different from that of the $Fm\bar{3}m$ structure, physical properties should in principle be obtained by averaging the results calculated from each snapshot instead of by directly calculating the property from the averaged structure. Such an effect can be seen from both Figs. 2(b) and 2(c) for the band gap and from Fig. 5 for the TE properties.

D. Effect of liquidlike cations on defect properties

We next study the defect properties in Cu_2Te and its solid solution with Ag_2Te. The Cu vacancy (v_{Cu}) is considered to be the main player that controls the hole concentration in these materials. We first show the problem caused by the liquidlike cations. In Fig. 6(a), we show the phonon spectrum of the AF-phase Cu_2Te calculated by PBE $+ U$ ($U = 7$ eV). Imaginary modes are seen in the whole Brillouin zone suggesting the instability of this phase. The standard approach to study a defect is to create a defect in a supercell and calculate its total energy.

However, for such an unstable system, the relaxed structure in this way will rely on the initial structure, as discussed below.

Taking v_{Cu} as the example, if the local defect structure preserves the high symmetry, one obtains a structure in Fig. 6(b). However, by carrying out a frequency calculation, 47 imaginary modes were found. By following these modes, low-energy structures will be obtained. The energy profile for these structures is shown in Fig. 6(d). Repeating this process, one may obtain a structure without exhibiting imaginary modes, similar to the structure as shown in Fig. 6(c). However, for such a complex structure, it is highly possible that the obtained structure is just metastable. Molecular dynamics simulation would be necessary for sampling the configuration space.

Figure 7(a) shows the evolution of the total energy of a supercell of Cu_2Te containing a v_{Cu} (E_D) over an MD simulation of 80 ps at 850 K. Figure 7(b) shows the distribution of the total energy. By adding the total energy of a Cu atom (E_{Cu}) in bulk fcc Cu, which was also obtained by an ensemble average over an MD simulation at 850 K, the energy $E_D + E_{Cu}$ can be compared with the average energy from a simulation on a perfect supercell without removing the Cu (E_0). The total energies can also be obtained by fitting the distributions in
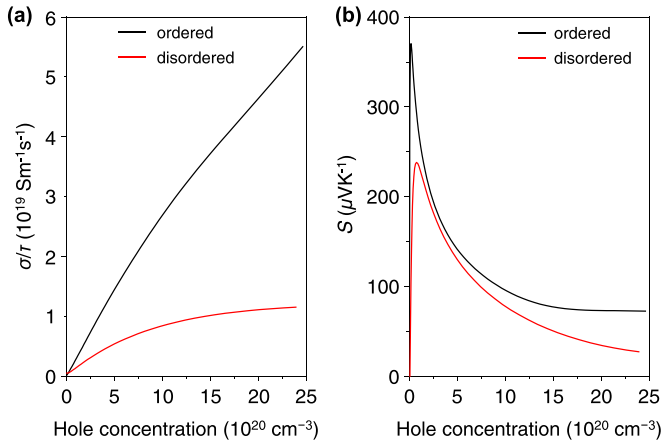
FIG. 5. (a) Ratio of electrical conductivity and relaxation time (σ/τ) and (b) Seebeck coefficient (S) of Cu_2Te as a function of hole concentration. The results for the ordered and disordered structures correspond to the band structures in Figs. 4(a) and 4(b), respectively.

Fig. 2(b) with Gaussion functions and then taking the peak values (marked by arrows), which will yield negligibly small difference from the ensemble averages. We carried out similar calculations for $Cu_{2-x}Ag_xTe$ with $x = 0.375$.

The calculated formation energies for v_{Cu} are shown in Fig. 7(c) as a function of MD simulation time. Different from the band gaps shown in Fig. 3(c), the convergence of the defect formation energy requires much longer MD simulation time. This is because the diffusive movements of the liquidlike cations renders it difficult to meet the ergodic requirement. In contrast, for displacive movements (i.e., each atom moves around a center), it takes a shorter simulation time to achieve convergence in MD-based calculations on defect properties [46]. The results in Fig. 7(c) based on 80-ps MD simulations suggest that Ag alloying could increase the formation energy of v_{Cu}, which is consistent with the experimental part of the
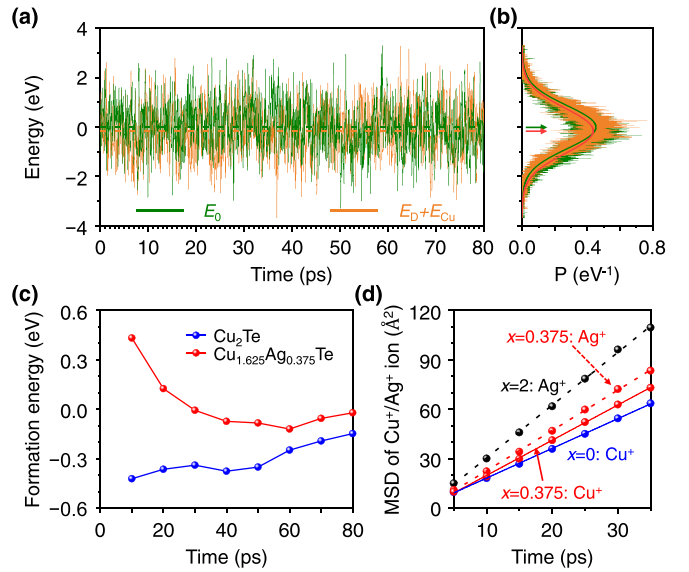

FIG. 7. (a) Evolution of the total energies of the defect-free supercell of Cu_2Te (E_0) and the supercell containing a v_{Cu} (E_D) over MD simulations of 80 ps at 850 K. E_{Cu} is the total energy of a Cu atom in bulk fcc Cu, which was also obtained by an ensemble average over an MD simulation at 850 K. The average of E_0 was set as the energy zero. (b) Distributions of total energies in (a). The arrows mark the peak values as obtained by Gaussian fittings (solid lines). (c) Defect formation energy of v_{Cu} in pristine Cu_2Te and $Cu_{1.625}Ag_{0.375}Te$ as a function of MD simulation time, over which the ensemble averages were carried out. (d) Mean-squared displacement (MSD) for Cu and Ag ions in Cu_2Te ($x = 0$), Ag_2Te ($x = 2$), and $Cu_{1.625}Ag_{0.375}Te$ ($x=0.375$).

previous work [11], namely, Ag alloying reduces the electrical conductivity of Cu_2Te. However, in the same work, there was a puzzle that the calculated formation energy of v_{Cu} was too negative (about $-1.2\,eV$). From Fig. 7(c), the formation
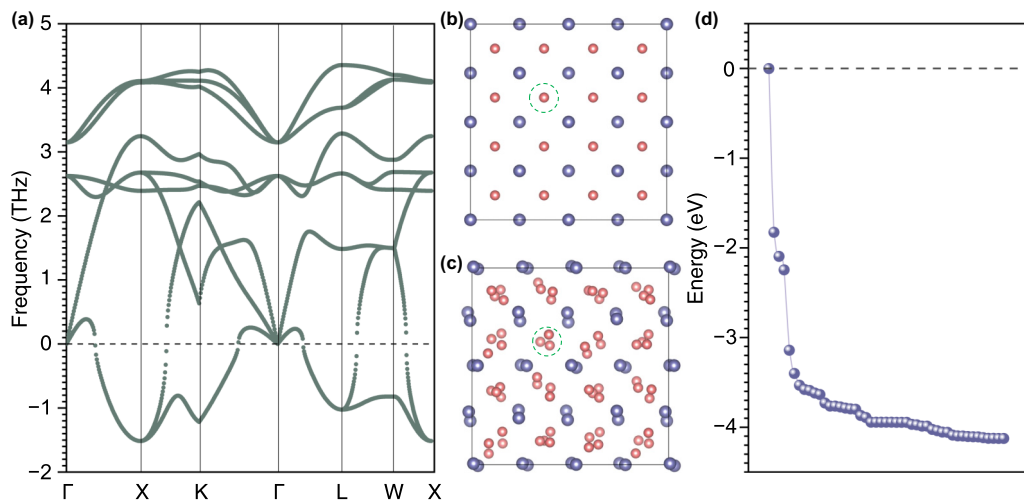

FIG. 6. (a) Phonon spectrum of Cu_2Te in the cubic antifluorite structure calculated by the PBE $+ U$ method with $U = 7\,eV$. The high-symmetry points in the Brillouin zone are shown in Fig. 2. (b) Relaxed structure of v_{Cu} in a supercell by preserving the high symmetry. The green dashed circle marks the position of the v_{Cu}. (c) The lowest-energy structure obtained by following the imaginary modes from a frequency calculation on the structure shown in (b). (d) Energy profile of the v_{Cu} defect structures by following all the imaginary modes from the structure in (b).

energy of v_{Cu} in pristine Cu_2Te obtained from MD simulations is about -0.15 eV. A negative formation energy always indicates thermodynamic instability, suggesting that the PBE $+ U$ method may still be subject to errors and more sophisticated methods such as HSE-base MD simulations need to be explored in future studies.

Finally, to illustrate the liquidlike behavior of cations, we show the MSD in Fig. 7(d) calculated by

$$\text{MSD}(t) = \frac{1}{N_{\text{step}}N_{\text{atom}}} \sum_{i=1}^{N_{\text{step}}} \sum_{j=1}^{N_{\text{atom}}} |r_j(t_i + t) - r_j(t_i)|^2,$$

where $r_j(t_i)$ represents the coordinates of atom j at time step t_i with i and j run over the number of MD steps and the number of atoms of interest (i.e., Cu or Ag in the present case), respectively. The good linearity of MSD as a function of t suggests the liquidlike behavior of the cations. By linear fitting, we can obtain the diffusion coefficient D by using $\text{MSD}(t) = 6Dt$, where the factor of 6 accounts for the three-dimensional diffusion. We considered Cu_2Te ($x = 0$), Ag_2Te ($x = 2$), and the case with $x = 0.375$. The calculated D is 3.0 and 5.3×10^{-5} cm^2/s for Cu and Ag ions in Cu_2Te and Ag_2Te, respectively. For the case with $x = 0.375$, the values (3.6×10^{-5} cm^2/s for Cu and 4.1×10^{-5} cm^2/s for Ag) are in between the two end members. These values are slightly higher than that for Cu_2Se (2.5×10^{-5} cm^2/s) experimentally measured at 622 K [47].

IV. CONCLUSION

We studied the effect of liquidlike cations on the electronic structure and defect properties of cubic AF-phase solid solutions $Cu_{2-x}Ag_xTe$. MD simulations provided interesting insights. Regarding the electronic structure, we found that the band-gap variation with increasing x obtained from ensemble average in MD simulations is much slower than that obtained by directly calculating from the high-symmetry ordered structures. Considering band-gap underestimation in PBE $+ U$ calculation, as compared with HSE $+ U +$ SOC calculation, the solid solutions within the whole range of x should exhibit significant band gaps. The liquidlike behavior of cations also results in flattened top valence bands, which reduce the Seebeck coefficient and electrical conductivity. Regarding the defect properties, we found that standard defect models employing the high-symmetry ordered structures with $Fm\bar{3}m$ space group can be easily trapped in unstable or metastable configurations due to the liquidlike behavior of the cations. MD simulations are necessary for sampling the configuration space. To obtain well-converged total energies in the defect calculations, significantly longer MD simulation time than that for converging the band gaps would be required. Our results suggest that Ag alloying could slightly increase the formation energy of Cu vacancy.

[1] Z.-H. Ge, B.-P. Zhang, Y.-X. Chen, Z.-X. Yu, Y. Liu, and J.-F. Li, Synthesis and transport property of $Cu_{1.8}S$ as a promising thermoelectric compound, Chem. Commun. **47**, 12697 (2011).

[2] H. Liu, X. Shi, F. Xu, L. Zhang, W. Zhang, L. Chen, Q. Li, C. Uher, T. Day, and G. J. Snyder, Copper ion liquid-like thermoelectrics, Nat. Mater. **11**, 422 (2012).

[3] B. Yu, W. Liu, S. Chen, H. Wang, H. Wang, G. Chen, and Z. Ren, Thermoelectric properties of copper selenide with ordered selenium layer and disordered copper layer, Nano Energy **1**, 472 (2012).

[4] S. Ballikaya, H. Chi, J. R. Salvador, and C. Uher, Thermoelectric properties of Ag-doped Cu_2Se and Cu_2Te, J. Mater. Chem. A **1**, 12478 (2013).

[5] Y. He, T. Day, T. Zhang, H. Liu, X. Shi, L. Chen, and G. J. Snyder, High thermoelectric performance in non-toxic earth-abundant copper sulfide, Adv. Mater. **26**, 3974 (2014).

[6] Y. He, T. Zhang, X. Shi, S.-H. Wei, and L. Chen, High thermoelectric performance in copper telluride, npj Asia Mater. **7**, e210 (2015).

[7] X. Su, F. Fu, Y. Yan, G. Zheng, T. Liang, Q. Zhang, X. Cheng, D. Yang, H. Chi, X. Tang, Q. Zhang, and C. Uher, Self-propagating high-temperature synthesis for compound thermoelectrics and new criterion for combustion processing, Nat. Commun. **5**, 4908 (2014).

[8] L. Zhao, X. Wang, F. Y. Fei, J. Wang, Z. Cheng, S. Dou, J. Wang, and G. J. Snyder, High thermoelectric and mechanical performance in highly dense $Cu_{2-x}S$ bulks prepared by a melt-solidification technique, J. Mater. Chem. A **3**, 9432 (2015).

[9] L.-l. Zhao, X.-l. Wang, J.-y. Wang, Z.-x. Cheng, S.-x. Dou, J. Wang, and L.-q. Liu, Superior intrinsic thermoelectric performance with zT of 1.8 in single-crystal and melt-quenched highly dense $Cu_{2-x}Se$ bulks, Sci. Rep. **5**, 7671 (2015).

[10] K. Zhao, A. B. Blichfeld, H. Chen, Q. Song, T. Zhang, C. Zhu, D. Ren, R. Hanus, P. Qiu, B. B. Iversen, F. Xu, G. J. Snyder, X. Shi, and L. Chen, Enhanced thermoelectric performance through tuning bonding energy in $Cu_2Se_{1-x}S_x$ liquid-like materials, Chem. Mater. **29**, 6367 (2017).

[11] K. Zhao, K. Liu, Z. Yue, Y. Wang, Q. Song, J. Li, M. Guan, Q. Xu, P. Qiu, H. Zhu, L. Chen, and X. Shi, Are Cu_2Te-based compounds excellent thermoelectric materials? Adv. Mater. **31**, 1903480 (2019).

[12] Y. Qiu, Y. Liu, J. Ye, J. Li, and L. Lian, Synergistic optimization of carrier transport and thermal conductivity in Sn-doped Cu_2Te, J. Mater. Chem. A **6**, 18928 (2018).

[13] X. Liang, D. Jin, and F. Dai, Phase transition engineering of Cu_2S to widen the temperature window of improved thermoelectric performance, Adv. Electron. Mater. **5**, 1900486 (2019).

[14] A. A. Olvera, N. A. Moroz, P. Sahoo, P. Ren, T. P. Bailey, A. A. Page, C. Uher, and P. F. P. Poudeu, Partial indium solubility induces chemical stability and colossal thermoelectric figure of merit in Cu$_2$Se, Energy Environ. Sci. **10**, 1668 (2017).

[15] R. Nunna, P. Qiu, M. Yin, H. Chen, R. Hanus, Q. Song, T. Zhang, M.-Y. Chou, M. T. Agne, J. He, G. J. Snyder, X. Shi, and L. Chen, Ultrahigh thermoelectric performance in Cu$_2$Se-based hybrid materials with highly dispersed molecular cnts, Energy Environ. Sci. **10**, 1928 (2017).

[16] P. Lu, H. Liu, X. Yuan, F. Xu, X. Shi, K. Zhao, W. Qiu, W. Zhang, and L. Chen, Multiformity and fluctuation of Cu ordering in Cu$_2$Se thermoelectric materials, J. Mater. Chem. A **3**, 6901 (2015).

[17] Y. Wei, P. Lu, C. Zhu, K. Zhao, X. Lu, H. Su, X. Shi, L. Chen, and F. Xu, Intrinsic lamellar defects containing atomic Cu in Cu$_2$X (X = S, Se) thermoelectric materials, J. Mater. Chem. C **9**, 4173 (2021).

[18] P. Lu, W. Qiu, Y. Wei, C. Zhu, X. Shi, L. Chen, and F. Xu, The order–disorder transition in Cu$_2$Se and medium-range ordering in the high-temperature phase, Acta Cryst. B **76**, 201 (2020).

[19] Y. Zhang, Y. Wang, L. Xi, R. Qiu, X. Shi, P. Zhang, and W. Zhang, Electronic structure of antifluorite Cu$_2$X (X = S, Se, Te) within the modified Becke-Johnson potential plus an on-site Coulomb U, J. Chem. Phys. **140**, 074702 (2014).

[20] O. M. Hussain, B. S. Naidu, and P. J. Reddy, Photovoltaic properties of n-CdS/p-Cu$_2$Te thin film heterojunctions, Thin Solid Films **193-194**, 777 (1990).

[21] B. S. Farag and S. A. Khodier, Spectral dependence of the absorption coefficient of thin films of nonstoichiometric Cu$_{2-x}$Te, Thin Solid Films **205**, 52 (1991).

[22] S. N. Mostafa, S. R. Selim, S. A. Soliman, and E. G. Gadalla, Electrochemical investigations of a copper-tellurium system and determination of the band gap for α-Cu$_2$Te, Electrochim. Acta **38**, 1699 (1993).

[23] D. Ferizović and M. Muñoz, Optical, electrical and structural properties of Cu$_2$Te thin films deposited by magnetron sputtering, Thin Solid Films **519**, 6115 (2011).

[24] Y. Pei, N. A. Heinz, and G. J. Snyder, Alloying to increase the band gap for improving thermoelectric properties of Ag$_2$Te, J. Mater. Chem. **21**, 18256 (2011).

[25] H. Zhu, J. Luo, H. Zhao, and J. Liang, Enhanced thermoelectric properties of p-type Ag$_2$Te by Cu substitution, J. Mater. Chem. A **3**, 10303 (2015).

[26] R. Wu, Z. Li, Y. Li, L. You, P. Luo, J. Yang, and J. Luo, Synergistic optimization of thermoelectric performance in p-type Ag$_2$Te through cu substitution, J. Materiomics **5**, 489 (2019).

[27] G. Kresse and J. Furthmüller, Efficiency of ab-initio total energy calculations for metals and semiconductors using a plane-wave basis set, Comput. Mater. Sci. **6**, 15 (1996).

[28] P. E. Blöchl, Projector augmented-wave method, Phys. Rev. B **50**, 17953 (1994).

[29] G. Kresse and D. Joubert, From ultrasoft pseudopotentials to the projector augmented-wave method, Phys. Rev. B **59**, 1758 (1999).

[30] J. P. Perdew, K. Burke, and M. Ernzerhof, Generalized Gradient Approximation Made Simple, Phys. Rev. Lett. **77**, 3865 (1996).

[31] J. Heyd, G. E. Scuseria, and M. Ernzerhof, Hybrid functionals based on a screened Coulomb potential, J. Chem. Phys. **118**, 8207 (2003).

[32] S. L. Dudarev, G. A. Botton, S. Y. Savrasov, C. J. Humphreys, and A. P. Sutton, Electron-energy-loss spectra and the structural stability of nickel oxide: An LSDA + U study, Phys. Rev. B **57**, 1505 (1998).

[33] M. Cococcioni and S. de Gironcoli, Linear response approach to the calculation of the effective interaction parameters in the LDA + U method, Phys. Rev. B **71**, 035105 (2005).

[34] S. Nosé, A molecular dynamics method for simulations in the canonical ensemble, Mol. Phys. **52**, 255 (1984).

[35] W. G. Hoover, Canonical dynamics: Equilibrium phase-space distributions, Phys. Rev. A **31**, 1695 (1985).

[36] A. Togo and I. Tanaka, First principles phonon calculations in materials science, Scr. Mater. **108**, 1 (2015).

[37] J. Yang, L. Xi, W. Zhang, L. D. Chen, and J. Yang, Electrical transport properties of filled CoSb$_3$ skutterudites: A theoretical study, J. Electron. Mater. **38**, 1397 (2009).

[38] Y. Sun, L. Xi, J. Yang, L. Wu, X. Shi, L. Chen, J. Snyder, J. Yang, and W. Zhang, The "electron crystal" behavior in copper chalcogenides Cu$_2$X (X = Se, S), J. Mater. Chem. A **5**, 5098 (2017).

[39] X. Li, Z. Zhang, J. Xi, D. J. Singh, Y. Sheng, J. Yang, and W. Zhang, TransOpt. A code to solve electrical transport properties of semiconductors in constant electron–phonon coupling approximation, Comput. Mater. Sci. **186**, 110074 (2021).

[40] R. Blachnik, M. Lasocka, and U. Walbrecht, The system copper-tellurium, J. Solid State Chem. **48**, 431 (1983).

[41] S.-y. Miyatani, S. Mori, and M. Yanagihara, Phase diagram and electrical properties of Cu$_{2-\delta}$Te, J. Phys. Soc. Jpn. **47**, 1152 (1979).

[42] M. C. Nguyen, J.-H. Choi, X. Zhao, C.-Z. Wang, Z. Zhang, and K.-M. Ho, New Layered Structures of Cuprous Chalcogenides as Thin Film Solar Cell Materials: Cu$_2$Te and Cu$_2$Se, Phys. Rev. Lett. **111**, 165502 (2013).

[43] W.-D. Liu, L. Yang, Z.-G. Chen, and J. Zou, Promising and eco-friendly Cu$_2$X–based thermoelectric materials: Progress and applications, Adv. Mater. **32**, 1905703 (2020).

[44] L. Yu, K. Luo, S. Chen, and C.-G. Duan, Cu–deficiency induced structural transition of Cu$_{2-x}$Te, CrystEngComm **17**, 2878 (2015).

[45] X. Wu, W. Gao, J. Chai, C. Ming, M. Chen, H. Zeng, P. Zhang, S. Zhang, and Y.-Y. Sun, Defect tolerance in chalcogenide perovskite photovoltaic material BaZrS$_3$, Sci. China Mater. **64**, 2976 (2021).

[46] X. Wu, C. Ming, J. Shi, H. Wang, D. West, S. Zhang, and Y.-Y. Sun, Defects in statically unstable solids: The case for cubic perovskite α-CsPbI$_3$, Chin. Phys. Lett. **39**, 046101 (2022).

[47] M. K. Balapanov, A. F. Nadejzdina, R. A. Yakshibayev, D. Lukmanov, and R. J. Gabitova, Ionic conductivity and chemical diffusion in Li$_x$Cu$_{2x}$Se superionic alloys, Ionics **5**, 20 (1999).